Trap-Dominated Nitrogen Dioxide and Ammonia Responses of Air-Stable *p*-channel Conjugated Polymers from Detailed Bias Stress Analysis

Tushita Mukhopadhyaya and Howard E. Katz*

Department of Materials Science and Engineering and Department of Chemistry, Johns Hopkins University, 206 Maryland Hall, 3400 North Charles Street, Baltimore, MD 21218, United States

*corresponding author: email hekatz@jhu.edu

Abstract

The improvement of conjugated polymer-based gas sensors involves fine tuning the backbone electronic structure and solid-state microstructure to combine high stability and sensitivity. We had previously developed a series of diketopyrrolopyrrole (**DPP**)-based polymer semiconductors by introducing a variety of fluorene linkers to study the trends and mechanisms governing gas sensitivities and electronic stability in air and under gate and drain bias stress. The proportional on-current change of organic field-effect transistors (**OFET**s) using a dithienyl **DPP**-fluorene polymer reached ~600% for a *sequential* exposure from 0.5-20 ppm of NO_2 for 5 minutes and also a high response-to-drift ratio under dynamic bias stress. In the present work we specify the roles of static bias stress and traps in the sensing process for the first time. Apart from electronic structure, defects at the molecular and microstructural levels govern the ability to form and sustain traps and subsequent backbone dopability. A polymer with a twisted backbone was observed to be capable of creating an energetically broad trap distribution while a polymer with a high degree of solid-state order shows a tendency to form an energetically narrow trap distribution and a fast passivation of traps on exposure to air. The stability and energetic distribution of traps on subjecting the polymers to bias stress was related to electronic structure and solid-state packing; and the ability of NO_2 and NH_3 to fill /create traps further was evaluated. At a bias stress condition of V_G=V_D=-80V, the polymers retain their NO_2 sensitivity *both post NO_2-aided recovery* and *air-aided recovery*. In order to verify the ability of NH_3 to create traps, *traps were erased from the OFET sensors by charging* with the aid of a positive gate voltage leading to an increase in the NH_3 response when compared to air controls. This work demonstrates that the charge-trap filling and generation response mechanism is predominant and can even be leveraged for higher responses to vapors. Backbone dopability appears to be a minor contributor to responses in this category of polymeric semiconductors with engineered defects. Finally, bias stress generally does not preclude this category of OFET vapor sensors from recovering their original sensitivities.

1. Introduction

Emissions of chemical pollutants such as NO_2 and NH_3 have posed increasing global environmental as well as health concerns, and therefore, gas sensing platforms or devices have been developed to yield responses to various gases in the environment for monitoring air quality, detecting gas emissions from industry, diagnosing diseases, etc.[1] Recently, polymer field-effect transistors (**FETs**) have been increasingly employed for vapor sensing because of certain advantages such as low operation temperature, tunable chemical structures and easy film and device fabrication methods.[2] Although relative to sensors based on inorganic semiconductors such as metal oxide, carbon nanotubes[3,4,5] or 2D materials[6,7], organic

semiconductor (OSC) gas sensors based on polymers have traditionally shown lower sensitivity, longer response/recovery time and high limit of detection (LOD), significant performance improvements have been achieved by optimizing solid-state thin film morphology, modulating conformation and backbone electronic structure, or by using improved device structures.[8,9,10,11] A library of polymer semiconductors used as gas sensors has so far been developed with a large degree of freedom to modify and tailor their structure and morphological structures which can also enable the construction of sensor arrays[12,13,14].

The fine-tuning of the chemical structure[15,16,17] and the optimization thin-film processing conditions[18] are essential to achieve a delicate balance between various parameters such as morphology[12], packing, orientation and charge transport to achieve the optimum sensing capability.[19,20] For example, many groups have implemented the concept of blends to achieve high specificity and optimal morphology and high surface area[21–25] for sensing.[26,27,28,29] Y. Kim *et al.* introduced modified graphene oxide/poly (9, 9′-dioctyl-fluorene-co-bithiophene: F8T2)-blend films for acetone and ethanol detection.[30] T. Xie *et al.* applied reduced graphene oxide/ poly(3-hexylthiophene) (P3HT) bilayer films for detection of nitrogen dioxide.[31] Bao *et al.* designed a microstructured dielectric in field-effect transistors, resulting in highly flexible monolithic transistor devices with excellent sensitivity.[10] Seo *et al.* systematically established that the increased grain boundary density of the organic semiconductor is beneficial for enhancing responses of the OFET gas sensor. At times, gases may only penetrate a small distance into a thicker film leading to a weaker response.[32,33,34,35 ,34]

Donor (**D**)–acceptor (**A**) copolymers possess certain advantages as compared to homopolymers, such as greater charge density tunability, larger effective conjugation lengths, polarized backbone leading to greater charge delocalization, ordered π-π stacking and high charge carrier mobilities which can be achieved by varying the strength of the donor and acceptor segments.[35,36] Recently, a variety of air stable **D–A** based polymer gas sensor devices have been reported.[37] A dikepyrrolopyrrole (**DPP)**-based **D−A** polymer with the −COOH groups in the side chains was used to construct a sensitive and selective **FET** sensor for ammonia by facilitating interactions between carboxylic acid and ammonia.[38] A (**DPP**)-based **D−A**-conjugated polymer PDPP4T-T containing H-bonding thymine groups was used for detection of CO and H_2S with high selectivity and sensitivity.[39] Zhang *et. al.* demonstrated porous sensors that exhibit enhanced sensitivity ~48.2%/ppm using an n-type polymer poly[N,N′-bis(2-octyldodecyl)-naphthalene-1,4,5,8-bis (dicarboximide)-2,6-diyl]-alt-5,5′-(2,2′-bithio-phene).[40] Katz *et. al.* reported a printable **OFET** sensor with sensitivity of 0.5 ppm v/v for ammonia and a conservative limit of detection of 0.1 ppm, using much more time- and cost-efficient processes than a vapor deposition.[41] Recently, the community has been paying increasing attention to the design of **D-A** polymers for achieving air stability along with optimum sensitivity.[42] Our group

recently reported a series of donor-acceptor **DPP** based polymers which show high signal to noise ratio alongside good response to oxidizing and reducing gases such as NO_2 and NH_3 respectively.[37] Air-stable ammonia sensing was also demonstrated for a series of isoindigo based polymers and a direct correlation was established with the thin film crystallinity. [18]

Contributions of bulk and interfacial defects, conformational inhomogeneity and packing effects to the mechanisms of gas sensing in the donor-acceptor semiconductor polymers have not been specifically determined.[43,19,44] Electronic traps in organic semiconductors can originate from structural defects or chemical impurities during or after the aggregation or crystallization process which can either be inherited or controlled through the growth and fabrication process.[45] Extrinsic traps can be intentionally or unintentionally introduced by temperature gradients, bias stress or by interfacing with dielectrics or other OSCs, or can happen due to transistor degradation.[46] In the bias stress effect, charge trapping occurs in deep, localized states in which carriers can be hardly released again on the time scales similar to charge transport. While hysteresis has been shown to correlate with traps generated at the channel-dielectric interface, semiconductor-ambient interface or localized at the contacts region,[47] the role of the immobile charges in the sensing process is still not thoroughly investigated.[2] Permeated gas molecules can act as trapping, trap-filling, or de-doping agents at the grain boundary, or if there is sufficient free volume, within a domain or grain.[18] In an unexposed film, carriers can transition from a conduction band into trap states imparting low conductivity.[48] Defects, therefore, can act as active sites which can be passivated by absorbing target gases and restoring free carriers, which restores the conductivity. Also, subtle physical and chemical effects at the interface affect the charge trapping; such as the presence of branching and chain ends greatly increasing the bias stress effect.[49] In addition, certain traps may be created in the interface between high-density or grains or aggregates and the dielectric which may be inaccessible by gases.[50,51] The sensing responses can also be a function of the operation voltage (i.e., V_{GS}) since at higher V_{GS}, most of the charge transport of a transistor takes place at the interface between the semiconductor and the gate dielectric layer, not in the bulk of the film. [52,53] Various interactions between injected analytes and the dielectric layer can also change the drain current of organic field-effect transistors (OFET)-based chemical sensors in the same manner as those between analytes and the semiconducting layer.[54–56] For enhancement of the sensitivity or selectivity, approaches such as UV irradiation, introduction of gas dielectric[57] and additional functionalization[58] at the semiconductor-dielectric interface have also been implemented.[59,60] Thus, while traps are typically regarded as an obstacle to achieving high performing semiconductor devices, they can also be exploited towards sensing as analytes modulate the trap density of states (DOS). The generation or passivation of charge carrier traps can thus be the predominant mechanism of sensing by polymers in OFETs. While designing

materials that can withstand static/dynamic bias stress, it is important to control molecule-based parameters (DOS and energy levels). A high highest occupied molecular orbital (HOMO) level (good aerial oxidizability) favours reversal of static bias stress. However, as seen for dynamic bias stress, easy oxidizability was seen to cause degradation and loss of environmental stability, expressed as noise.[37] *While moderate oxidizability has been seen to favour both good responses and low drifts leading to high signal to noise ratios, subtle physical and chemical effects at the interface and microstructural variables such as branching and chain ends greatly increases the bias stress effect.* In recent years; quantum chemical analyses of conjugated polymers based on fluorene with conformational and chemical defects arising from tetrahedral kinks and ring torsional defects around the thiophene-phenyl bond were done; these were reported to localize the electron−hole excitation in one segment of the polymer chain due to disruption of backbone planarity. [61,62,63] The macrostructural order of the fluorene-based homo- and alternating copolymer thin films have been revealed by X-ray diffraction (**XRD**) scans corresponding to large *d*-spacings with broad statistical distributions, and are in good agreement with the length of the bulky dioctyl groups that are oriented perpendicular to the main chain of the polymer.[64,65,66] The typical π-π stacking distances of ∼4.2–4.4 A˚ have been previously reported in *fluorene-based polymeric and oligomeric semiconductors* which is indicative of poor lamellar packing. On the other hand; *diketopyrrolopyrrole (**DPP**)-bithiophene* based polymers have been shown to exhibit *d*-spacings ∼1.9 nm and π-π stacking distances of ∼0.4 nm.[67,68] The poor crystallinity of the **DPP**-fluorene copolymers[69] also reflect in their blue-shifted steady-state UV-visible spectra (**PF1-PF4**) as compared to that of **P6**. Greater effective backbone planarity favours greater backbone delocalization, which raises the **HOMO** energy (refer to **CV** studies) as seen for **P6** followed by **PF4**, while the deepest **HOMO** was for **PF2**.[37] To corroborate this, our bias-stress quantification revealed that **PF2** has a broader distribution of trap energy than that of **P6**; which is a consequence of difference in structural defect densities. Thus, optimization of microstructure by controlling *structural parameters* such as side-chain and backbone architecture (effective crystallinity) and the *electronic structure* variables such as density of states (**DOS**) near the band edge enables stability to static bias stress.[70,54]

Based on this; we now consider the relative roles of traps and backbone electronic structure and their respective contributions to the mechanism of response to oxidizing and reducing gases by the polymers shown in **Figure 1**. We had observed in a previous study that the defects played an important role in determining the ratio of responses on exposure to NO_2 and NH_3 to the drifts on taking the device through repeated gate voltage sweeps during dynamic bias stress.[37] A high charge carrier density and greater delocalization throughout the backbone led to high responses (up to 600%) combined with good environmental stability contributing to high signal to drift (D) values.[37] In contrast to the *dynamic* bias stress procedure from repeated gate

voltage cycling that we used in our previous study, we hereby examine the effects of *static* gate bias on the reproducibility of polymer **OFET** sensors and also elucidate the relative roles of traps and carrier densities in the gas sensing mechanism[49,62,63,73] by (i) subjecting the polymers to bias stress during and followed by exposure to NO_2 and NH_3 and (ii) bias stress followed by electrostatic doping ("reverse bias stress") and subsequent exposure to NH_3 and NO_2. *The stability of polymer **OFETs** under static bias stress under high voltages, used in this work, is essential to be evaluated, as under practical operating conditions the device would often remain in the 'on' state.*

The novelty of the present work is as follows: (a) the energetic distribution of the charge traps and the capability of creating them in the polymers are studied as a function of backbone structure. Our results reveal that **PF2** is capable of creating an energetically broad distribution of traps (consistent with our previous study with this polymer on dynamic bias stress) while **P6** creates a narrow distribution of traps. A larger, stable shift in V_{th} during the static biasing process in this work indicates the presence of deep traps or localized states within the grain boundaries; the density of which is higher in **PF2** as indicated by morphology studies (atomic force microscopy, **AFM**). (b) The ability of analyte vapors to passivate and create traps, and release carriers was monitored by recovery time after bias stress in the presence and absence of the vapors, illustrating the role of the traps in the vapor response under different conditions. Recovery from bias stress, in the ambient atmosphere, is the fastest for **P6** while **PF2** shows the least tendency to refill the created traps when exposed to air for similar time scales as NO_2 exposure, which accelerated the recovery. This is a signature of the spiro substitution (defect) in **PF2,** which impairs effective π-π stacking and inhibit the close packing of the polymer chains.[37] In contrast to **PF2, PF4** has additional thiophene linkers which helps overcome the ortho hydrogen repulsions between **DPP** and fluorene derivative. **P6** shows enhanced intermolecular interaction and high degree of planarity and π-π stacking. The electronic structures of P6 (revealed by cyclic voltammetry) reveal easy and facile backbone oxidizability (a high HOMO level) and therefore easily exhibits drifts even in air. Thus, **PF4** is a compromise between the extremes (in terms of structural defects) of **PF2** and **P6**, explaining its optimal D value, even though it does not recover from bias stress as rapidly as **PF6**. **PF2**, on the other hand, showed the greatest enhancement in response to ammonia after reverse bias stress. (c) Since improving the device reproducibility is also of crucial importance for achieving practical applications of **OFETs,** subjecting **OFET** gas sensors to static bias-stress enabled us to, for the first time, test the sensors' ability to withstand the effect of extended bias stress and the effect of this bias stress and subsequent recovery on gas response. We did this using a novel application of p-values to show excellent reproducibility of responses before and after bias stress.

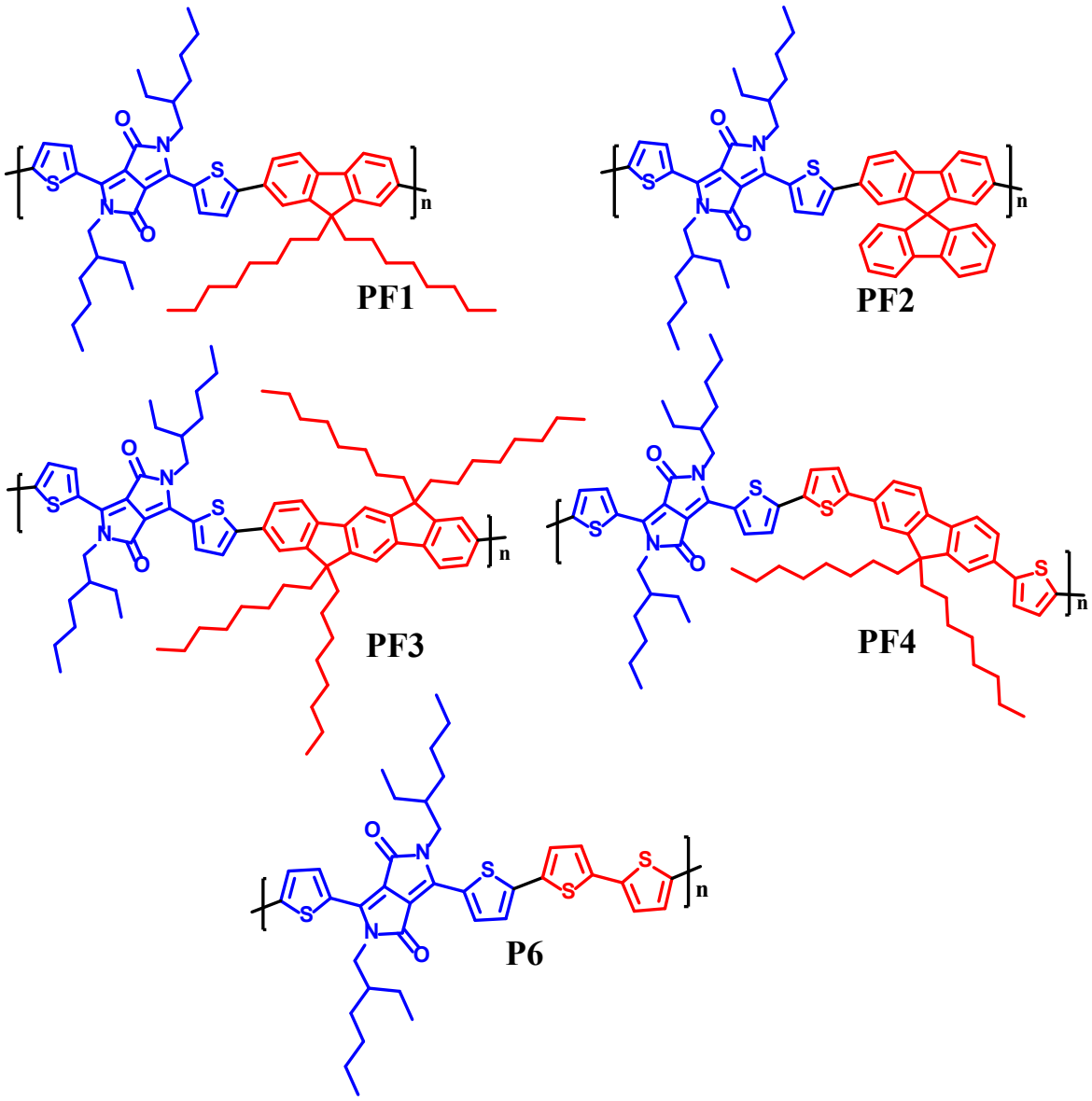

Figure 1. Molecules of interest

Results and Discussion. The synthesis and characterization data (^{1}H NMR and Gel Permeation Chromatography (**GPC**)) are shown in **Figure S1-S9, SI** and **Table S1, SI**. The cyclic voltammograms (**PF1-P6**) are reprinted in **Figure S10, SI**. The effects of structural modifications on the oxidation potential (highest occupied molecular orbital (**HOMO**) of the polymers were evaluated by cyclic voltammetry of the polymers in solution. Pt was used as the working electrode and Ag/AgCl as the reference electrode in 0.1 M tetrabutylammonium tetrafluoroborate acetonitrile solution with a scan rate of 0.5 V s^{-1} and the tests were calibrated using a ferrocene/ ferrocenium redox couple. **PF1**, **PF3** and **PF4** show quasi-reversible two-electron oxidation cycles, indicating the participation of the fluorene and thiophene donor chromophores in the oxidation process. **P6** shows a one-electron reversible oxidation cycle

which indicates a greater delocalization of the **HOMO** levels in **P6** leading to higher oxidizability. The **HOMO** levels extracted from the onsets of the oxidation waves in the CV data are -5.37 eV, -5.47 eV, -5.29 eV, -5.19 eV, and -5.12 eV for **PF1-P6**; which reveal that the **HOMO** levels of **PF1**, **PF2**, and **PF3** are deeper compared to those of **PF4** and **P6**. **OFET**s were fabricated in the top-contact, bottom-gate architecture. Output and transfer curves are shown in **Figure S11, S12, SI** respectively. The original devices without gas exposure show typical *p*-type transport. The *p*-channel mobilities and the threshold voltages (V_{th}) of the transistors are collected in **Table S2, SI**. **P6** exhibits the highest hole mobility of 0.12± 0.02 $cm^2V^{-1}s^{-1}$. **PF3** shows p-channel mobility of ~ ($1.2x10^{-3}$) ± ($7x10^{-4}$) $cm^2V^{-1}s^{-1}$ while films of the other four polymers exhibit much lower hole mobilities ~$2.0x10^{-4}$ $cm^2V^{-1}s^{-1}$. V_{th} values (**Table S2, SI**) of the polymers containing the fluorene spacer are higher than those of **P6.** In our previous work, the responses to a given NO_2 and NH_3 concentration were measured after subjecting the sensors to repeated gate voltage sweeps (~25 cycles). The transfer curves (and the changes in I_{DS} (%)) for optimized devices for NO_2 and NH_3 exposure are shown in **Figure S13-S15 (SI)**.[37] **Figure S15, SI** also shows the 25 scans that preceded the response observations as an example of dynamic bias stress. The key findings from our previous work were that the effect of the drifts is smaller than the NO_2 response (except for **PF2**) and is also smaller than that of the static bias stress employed in the present work. Once an initial trap distribution is established by a few excursions to high V_g, further creation of traps by dynamic bias stress from additional sweeps is not very prominent.[74,75] *Please note that in the previous work, we exposed devices stepwise (or in a ramped fashion) to concentrations of 0, 0.5,1,2,3,5,10,20 ppm and monitored the responses at -80 V, -60 V and V'= (V_{th}-40) V.*[37] *In this study, we directly expose the sensor to 10 ppm of NO_2/NH_3 and monitor all responses at V_G=-80 V. It is noteworthy to explore the role of contact resistance in vapor sensing. We varied the length of the channel (width constant) for **P6** with data reported in **Figure S16, SI**. The effect of varying channel lengths on NO_2 (10 ppm) sensing is shown in **Figure S16 (b), (c), (d), SI** (best devices). An average over 3 devices (for each channel length) revealed that the response~170±20% (measured at V_G=-80 V) is independent of the length of the channel, and contact resistance is too negligible to affect the response.*

This main section is organized into three parts. First, we perform a detailed analysis of the bias stress behavior of the polymers themselves. We then investigate the effect of conventional bias stress (maintaining accumulation regime V_{GS}) on responses to vapors. Finally, we consider the effect of reverse bias stress (electrostatic doping) on the responses.

Polymer bias stress effects. We subjected the OFETs to bias stress under the condition V_G=-80 V, V_D=-80 V for 5 hours or 18000 seconds (**Figure 2, Figure 3**). In this case the average bias voltage in the channel is -40 V. It is noteworthy that under static bias stress, the changes

reflected in the transfer curves during the process of trap creation are not uniform over the 300 minutes or 5 hours' time interval. The bias stress in our experiment was applied in the linear regime and the I_{DS} and ΔV_{th} evolution can be fit to a stretched exponential function

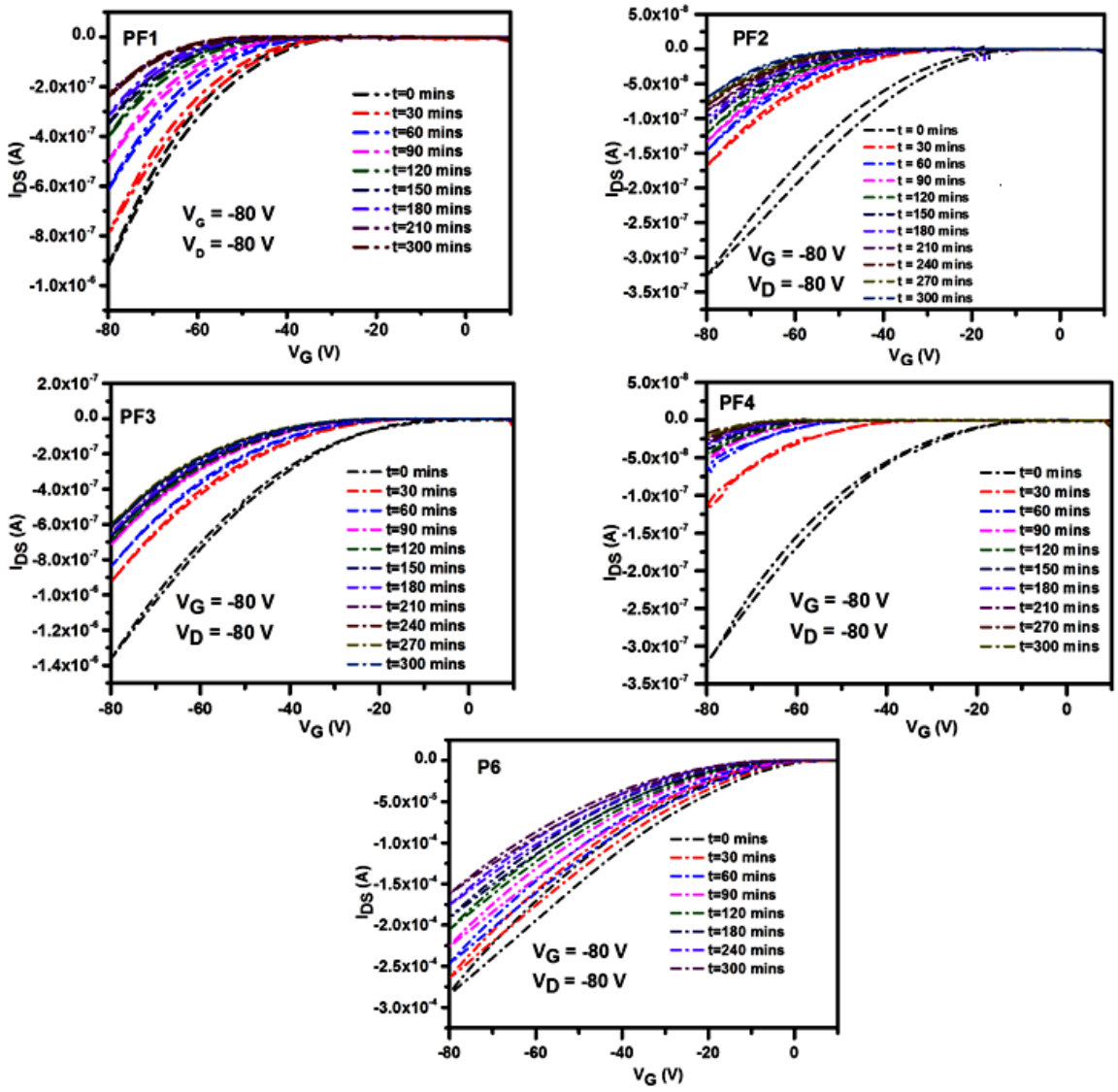

Figure 2. Transfer curves recorded at regular intervals of time for **PF1-P6** during bias stress application process (V_G=V_D=-80 V, time=18000 seconds)

$I_D(t)=I_0(0)\exp[-(t/\tau)^{\beta}]$ or $\Delta V_{th}=(V_{th,0}-V_{G,bias})[1-\exp\{-(t/\tau)^{\beta}\}]$.[76] The parameters were obtained by fitting the logarithmic form of the equation as explained in SI on page 10. The trapped hole carriers quantity q shows an increase with time that causes the rate of charges migrating to the drain electrode (I_{DS}), to decrease. The parameters β and τ express the rate at which the threshold voltage shifts during bias stress. We have extracted the β and τ values both from the continuous ΔV_{th} versus time decay (**Figure 4**) and the discrete transfer curves of **Figure 2** (**Figure 5, Table 1**). The fits from the ΔV_{th} vs. time graphs are shown in **Figure S17, SI** and the values are collected in **Table 2**.

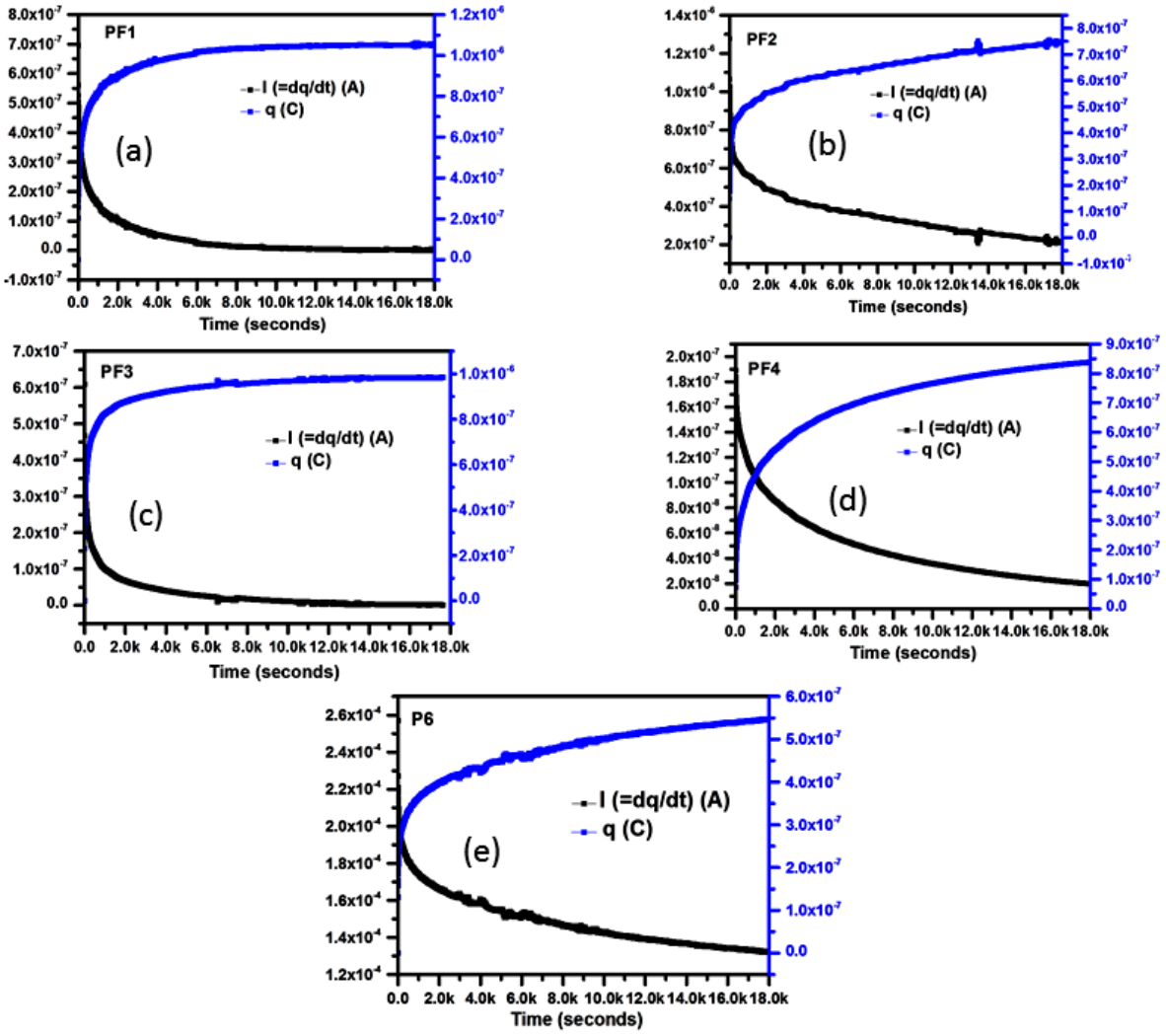

Figure 3. Plots of I_{DS} versus time (in black) and q versus time where q is calculated as C_{ox} (F)* ΔV_{th} (shown in blue). Here, the bias stress condition is V_G=V_D=-80 V and the application time is 18000 seconds (5 hours).

The values summarized in **Table 1** and **Table 2** are in qualitative agreement with each other. While the β values extracted from the transfer curves are slightly larger, the agreement shows that a similar electronic transformation occurs during both procedures. The larger τ values indicate longer time for charge trapping for a narrow range of trap energies. As also seen in our previous study, **PF2** and **PF3** showed the largest drifts on being subjected to dynamic bias stress, because of their high free volume and aggregation patterns.[37]

The stretching parameter β close to 1 indicates a narrow distribution of time constants (the limit β = 1 being the exponential function with a single time constant), while a smaller stretching parameter (β < 1) implies a broader distribution of time constants.[52] From **Table 1,** it is revealed that the bias stress reveals a broader range of activation energies for **PF2** and the narrowest for P6 based on the above analogy. This observation is consistent with steady-state

UV-visible studies that the bulky and spiro subunits impair effective π-π stacking and inhibit the close packing of the polymer chains[77,78] while **P6** has a high degree of order and π-π stacking.[79]

Table 1. β and τ values for **PF1-P6** (V_G=V_D=-80 V), with trap energy breadths in parentheses (k_bT/β) in eV (extracted from **Figure 2**)

Polymers	β	τ (mins)
PF1	0.43 (0.07 eV)	335
PF2	0.35 (0.09 eV)	521
PF3	0.43 (0.07 eV)	501
PF4	0.67 (0.04 eV)	510
P6	0.96 (0.03 eV)	1373

Table 2. List of β and τ (obtained from **Figure S17, SI**). (k_bT/β) (eV) are indicated in parenthesis

Polymers	β	τ (mins)
PF1	0.44 (0.06 eV)	435
PF2	0.27 (0.11 eV)	620
PF3	0.31 (0.09 eV)	605
PF4	0.42 (0.07 eV)	634
P6	0.69 (0.05 eV)	1052

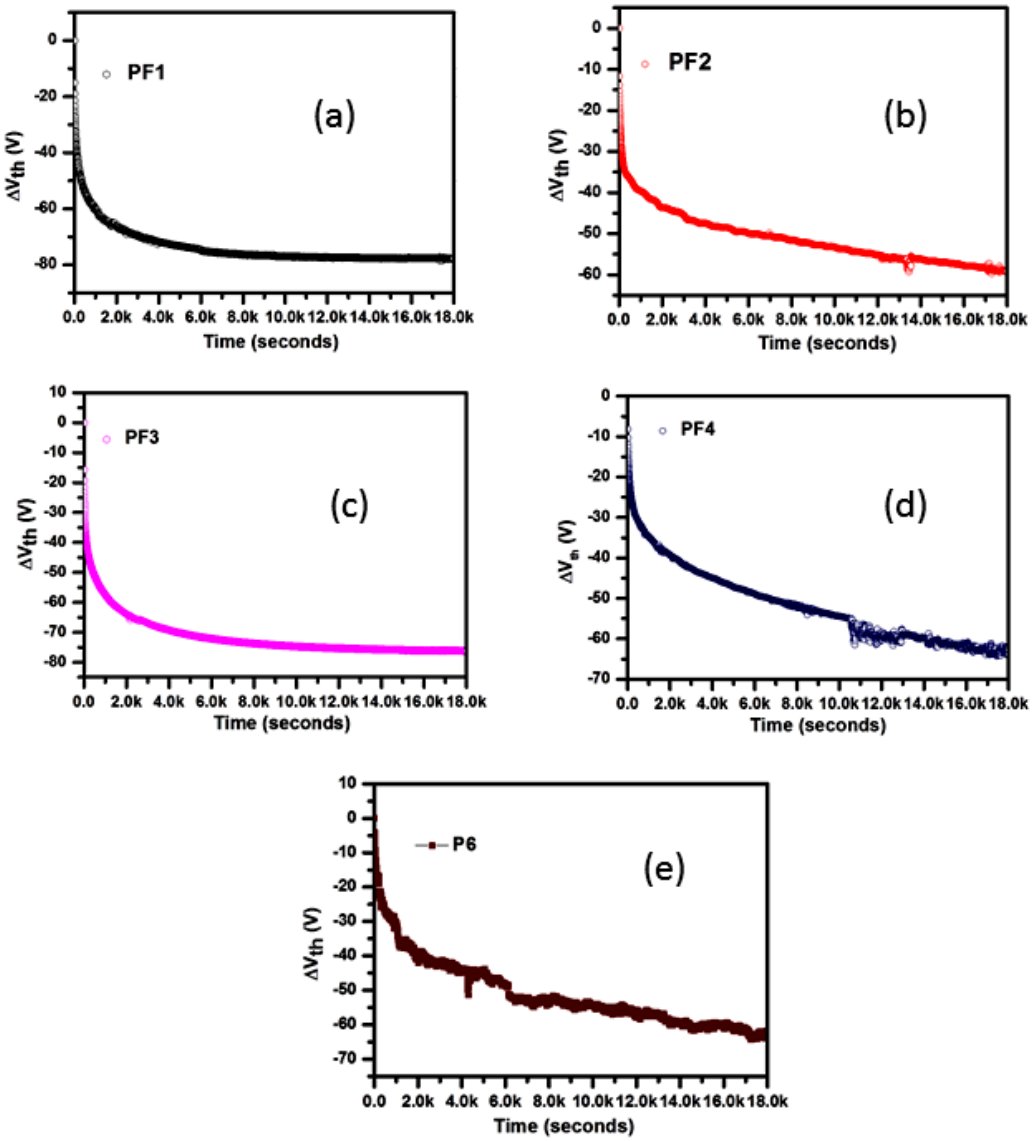

Figure 4. ΔV_{th} versus time (seconds) plot for the bias application process (V_G=-80 V, V_D=-80 V) for 18000 seconds (5 hours)

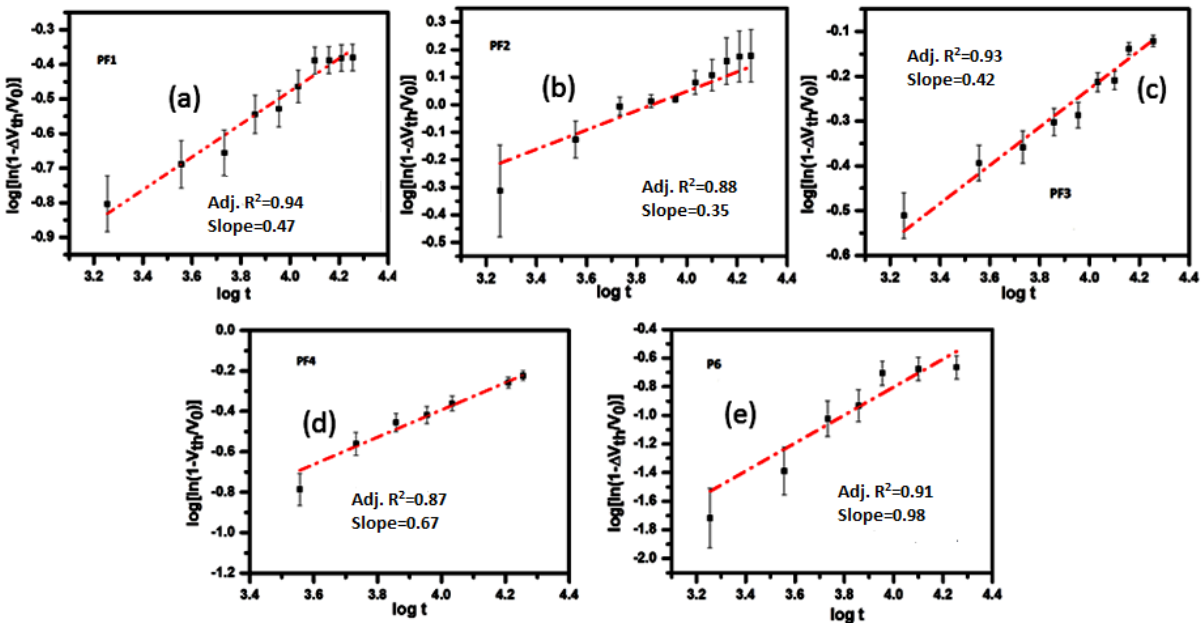

Figure 5. Fits of log[ln (1-$\Delta V_{th}/V_0$)] versus log t (using the transfer curves in **Figure 2**) to extract β and τ values**.**

The subthreshold slopes (**SS**) (dlog (I_{DS})/dV_G)$^{-1}$ at ambient temperature are 18000, 36000, 17000, 18000, 4000 mV/dec for **PF1**, **PF2**, **PF3**, **PF4** and **P6**. The slope of the subthreshold region is determined by the deep traps.[80,81] A high degree of order in the **OFETs** reflects as very steep subthreshold region and a high mobility (as seen for **P6**), whereas in the evaporated devices in general, the subthreshold is broad and the mobility is lower. Substituting N(interface) as ~C_iV_{th}/e, we can obtain the interfacial trap density per unit area per unit energy which is a measure of shallow trap densities. Since the sub threshold region is defined by $V_{GS} < V_{th}$, the intragrain effects are more predominant in this voltage and hence the **SS** method probes deeper band gap states than the V_{th}.[45] Therefore, **PF2** has the highest deep band gap states while **P6** has the lowest as evident from the **SS** values in our polymer series. The differences in **SS** arise because of different film microstructures characterized by small grains and large grains. The largest bulk trap density of **PF2** correlates with the smaller grain sizes and porous morphology by **AFM** and poor film coverage as described before in our previous work.[39] (**AFM** data are discussed again in **Figure S20, SI**.) **Table 1** reveals the interface trap densities at room temperature (294 K). We observe that irrespective of the backbone design, the differences in interface trap densities among the polymers are quite modest.

Figure S18, S19, SI depicts the transfer curves and plots of lnμ versus 1/T (K^{-1}). The trap energy (E_a) was extracted from the mobility-temperature (μ–T) relationships. According to the Arrhenius equation, μ α exp (-E_a/k_bT) where k_b represents Boltzmann constant. The trap potentials are: 0.09, 0.1, 0.1, 0.1 and 0.07 eV for **PF1**, **PF2**, **PF3**, **PF4** and **P6** respectively. The

values have been extracted by fitting the points; with error bars; by measuring mobilities corresponding to each temperature (for an individual polymer) from at least 3 devices. The correlation coefficients R^2 are between 0.9 and 0.1. The standard errors in the slopes are close to 25%, except for **P6,** for which it is closer to 50%, but still giving a comparable trap potential. The trap energy magnitudes are higher than the room temperature activation energy (~0.03 eV), indicating that the concentrations of trapped carriers in these polymers are significant. Trap energies of ~0.1 eV or deeper are indicative of traps far below the extended states. During the bias stress, molecular rearrangement can take place in the grain boundaries resulting in localization of electronic states with increased density of deep traps. Deep traps can also be located within the dielectric layer.[49,82] A poor thin film coverage and surface bonding defects (as in α-Si [83,84]) can also contribute to deep traps.[85,86]

The degree of solid-state order manifested itself as free volumes (**DSC** measurements) yielded values 9.10%, 9.12%, 9.33%, 8.50%, and 8.51% respectively (**PF1**-**P6**) at the device annealing temperature of 120°C used for the sensor **OFET**s. The free volumes have been earlier elucidated and reported in our earlier study (**DSC** measurements). The percentage free volume at a given temperature of the polymers from the **DSC** measurements using the equation ($V_{free:exs, SB}/V$) ≈ ($\alpha_L - \alpha_G$)T where α is the coefficient of thermal expansion in the liquid (L) and glassy (G) states and $V_{free:exs, SB}/V$. Since ($\alpha_L - \alpha_G$) ~$0.113/T_g$, the percentage free volumes can be estimated as 9.10, 9.12, 9.33, 8.50, 8.75, 8.51, and 10.43% at the device annealing temperature of 120 °C used for the sensor **OFETs**.[87,88,37] Although identical side chains have been incorporated in all the polymers, the backbone design helps modulate the free volume by controlling the density of side chains and chain ends which is a function of the degree of backbone twist or conformation. **PF1, PF2**, and **PF3** have higher free volumes than **PF4** and **P6,** correlated with number densities of side chains. The side chain bulkiness and density are known to impede efficient π-π stacking. The Atomic Force Microscopy (**AFM**) images are shown in **Figure S20, SI**. Films of polymers **PF3**, **PF4**, **P6** exhibit more continuous grains and better coverage which reflects in their low root mean square roughnesses (r.m.s.) of 0.56 nm, 2.74 nm, 1.72 nm respectively; which aids charge transport. **PF1** and **PF2** exhibit lesser surface coverage and smaller grains connecting the grains and possess r.m.s. roughness of 4.25 nm, 6.79 nm, 0.562 nm and 5.88 nm respectively. A smoother film surface topology is associated with lesser traps and grain boundaries and hence, higher *p*-channel mobilities.

Table 3. Summary of values of N(interface) with respect to temperature ($m^{-2}V^{-1}$).

Polymers	294 K	323 K	373 K
PF1	1.30E16	5.05E15	3.70E15
PF2	6.90E15	8.25E14	1.72E15
PF3	9.56E15	4.36E15	1.80E15
PF4	6.30E15	6.25E15	5.67E15
P6	6.43E15	4.46E15	3.90E15

The trends in β and τ, both in the discrete and continuous case, show similar trends with respect to the electronic structure and solid-state microstructural aspects in accordance with (i) **PF2** has thin film voids and poor packing/aggregation manifesting as large free volumes (ii) **P6** has the highest degree of microstructural order and larger concentration of mobile holes as seen from V_{th} and μ values and low free volumes and high grain density. Films **PF3**, **PF4** and **P6** are more continuous than **PF1** and **PF2** based on lower root mean square roughnesses (r.m.s.) (as shown before). On the other hand, higher roughness (from grain boundaries and voids) is associated with a high number density of deep traps.

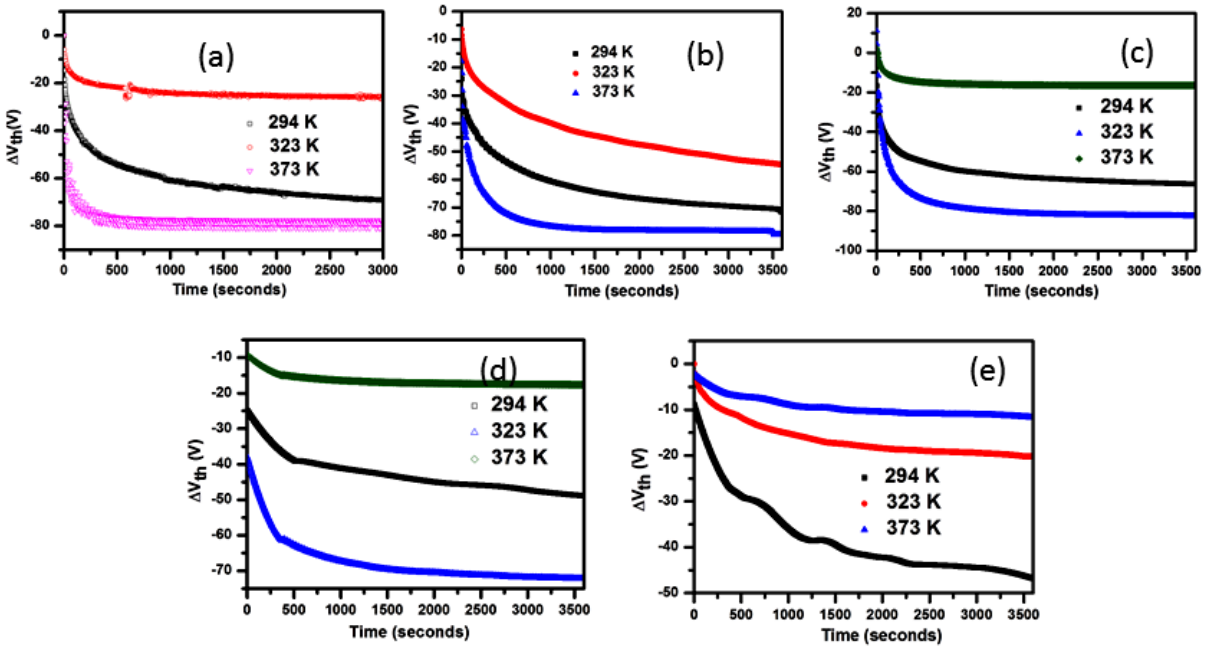

Figure 6. Temperature dependent gate bias measurements (294 K, 323 K, 373 K) for (a)-(e) **PF1-P6**. V_G=V_D=-80 V.

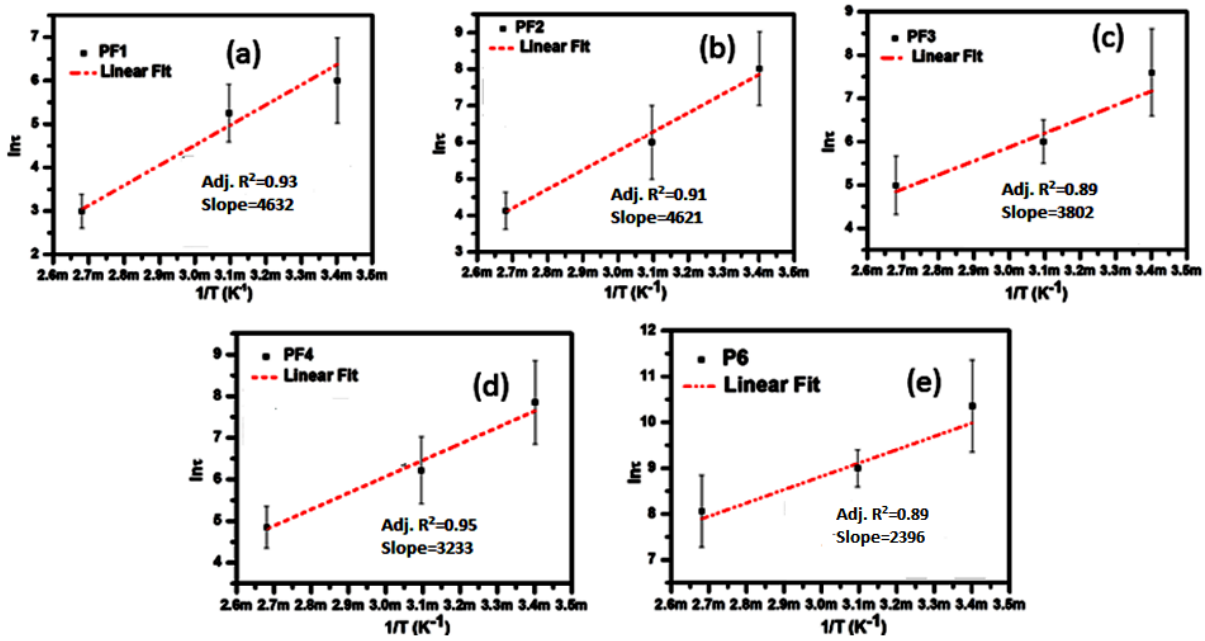

Figure 7. Plots of lnτ versus 1/T (K^{-1})

The parameter τ has Arrhenius-type temperature dependence. $\tau = \nu^{-1} \exp(E_a/k_bT)$ where ν is the frequency prefactor, E_a is the mean activation energy of trapping, k_b is the Boltzmann constant and T is the absolute temperature. Decay profiles are shown in **Figure 6.** To further

analyse τ, we measured τ at 294 K, 323 K and 373 K; the Arrhenius plots are shown in **Figure 7.** The slope and y-intercepts of the linear fits correspond to E_a and -ln ν, respectively. Extracted values are summarized in **Table S3, SI**. The resulting E_a is dependent on the polymer structure and the solid-state thin film microstructure. The frequency prefactor ν is a trap attempt frequency that is proportional to the density of trap sites in which charge carriers are prone to be trapped under bias stress; ν decreases as conformational and structural order increases. The value of ν for **PF1** is the highest which corresponds to a high density of trap sites, while **P6** has many fewer. While at first glance, this suggests a certain superiority for **P6**, it is also possible that a deficiency of sites where bias stress trapping could occur could lead to increased drift in the environment detrimental for sensing, as an OFET stabilized after bias stress might be less prone to trapping by environmental contamination, an observation that was also noted for **P6.**[39] The reason for lesser drift in **PF4** is presumably related to the apparent slower trapping processes in these polymers. **PF4** is characterized by relatively low free volume and a seemingly optimal oxidizability, less facile than **P6** and easier than the others. In contrast, the energy barrier to occupying each trap site can be described in terms of E_a. It has been reported that the energy structures of trap sites and their creation by bias stress are strongly affected by the chemical nature of semiconductors and gate-dielectric,[80,89,90,91] The E_a values are in order of the oxidation potential as seen from **CV** studies (**Figure S10, SI**). On short time scales, there could be an optimum E_a for trap filling that could stabilize a device while a vapor response is recorded. For completeness, we also monitored the change in mobility during these experiments (**Figure S21, SI**). For most of the experiment time (15,000 seconds), mobility changed on the order of 20% or less, and had a relatively minor effect on I_{DS} compared to $V_{th.}$

Relationship between bias stress-induced traps and response to vapors: We used the bias stress platform to separate the effects and relative weights of the trap-filling, doping, and impact of the electronic energy levels and solid-state microstructure on responses to vapors. We chose 10 ppm as the gas concentration (for V_G=V_D=-80 V). *In this study, the responses (% change in I_{DS}) are with respect to V_G=-80 V (from transfer curves) and all exposures are at 10 ppm directly, as opposed to cumulative exposures in steps in the previous work. Also, after the bias stress and recovery processes, when the retention of sensitivity is checked, the time is fixed to 5 minutes in accordance with the exposure time (=5 minutes for every gas concentration) in our previous work.*[37] It is also imperative to note that although we had previously monitored the sensitivity (%) and 'D' values as a function of gate voltage (the most comparable response being obtained at (V_{th}-40) V); in this study we elucidated all responses at a fixed voltage of V_G=-80 V.

Figure 8 compares the ability of the polymers to create traps during bias stress under different environments, (i) air (ii) NO_2 (10 ppm) and (iii) NH_3 (10 ppm), as assessed by evaluations of I_{DS} (A) decay. Fittings are shown (for NO_2 and NH_3 atmosphere) in **Figure S22**, **S23, SI** and the parameters are collected in **Table S4, SI**. Alternatively, $\beta=T/T_0$ where T_0 is the characteristic energy of traps [52,71,92] and a measure of trap activation energy distributions. The larger values of T_0 (lower β values) are indicative of the range of rate constants of the trap creation process. The τ values under NO_2 atmosphere are 600 mins, 280 mins, 313 mins, 1155 mins, and 1167 mins for **PF1-P6**. The τ values under NH_3 atmosphere are generally lower at 240 mins, 282 mins, 125 mins, 560 mins, and 248 mins for **PF1-P6**, similar to those in air and lower than for NO_2, except for **PF2**. This implies NO_2 slows the trap creation process as compared to NH_3 and air. It can be seen that under an oxidizing atmosphere, the rate constant for trap creation ($k=1/\tau$) follows the

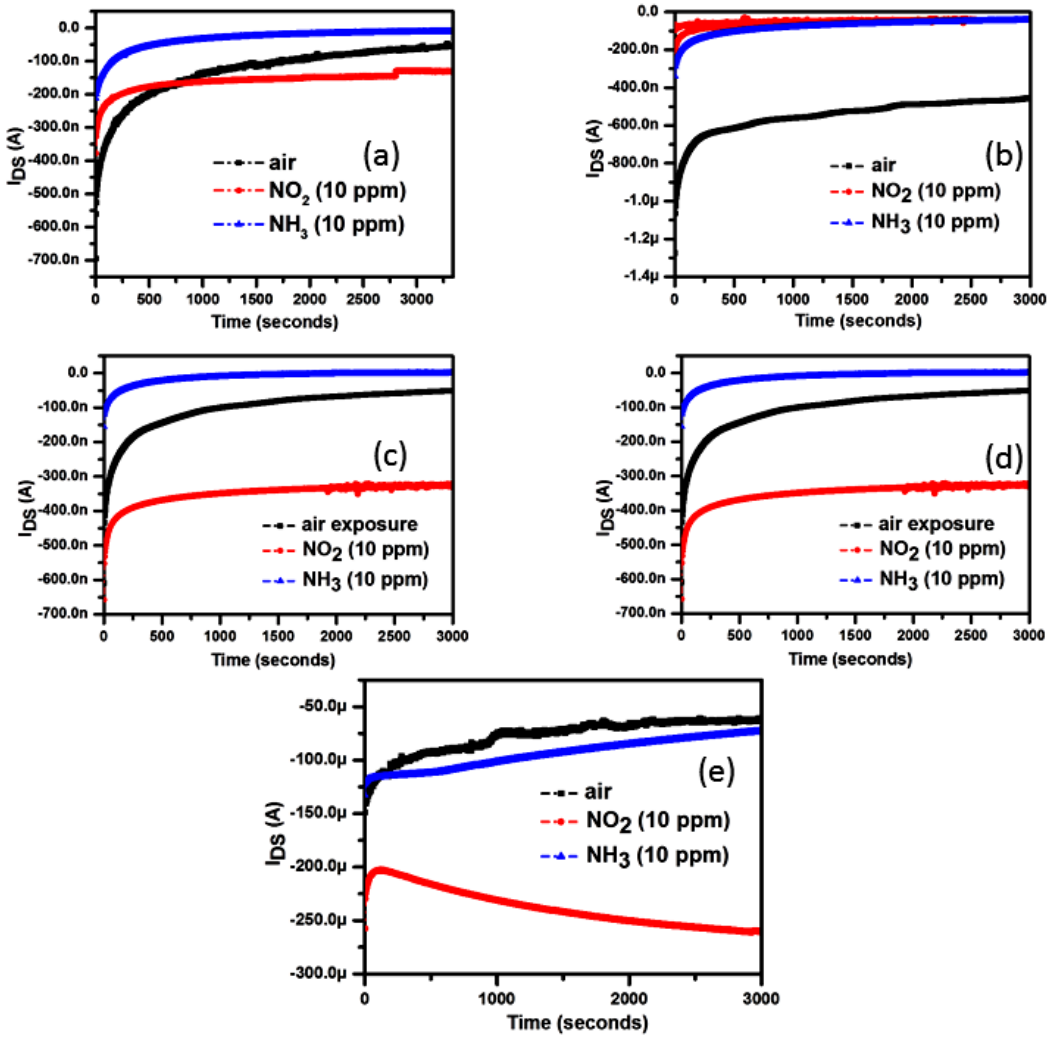

Figure 8. I_{DS} (A) decay versus time (seconds) under (i) air (ii) NO_2 (10 ppm) (iii) NH_3 (10 ppm) (environments). (a) **PF1** (b) **PF2** (c) **PF3** (d) **PF4** (e) **P6**. The duration is 1 hour. The choice of 1 hour is based on the observation that most polymers achieve a curve flattening in this time duration; therefore the number of points obtained from the plot would be enough to obtain the initial values of β and τ.

order of oxidation potential (CV) or electron donating ability of the polymers (**PF1-P6**). This also provides additional interpretation of our earlier observation of a weak response to NH_3 under conditions of dynamic bias stress; the response only slightly perturbs the trap formation process induced by bias stress in air (discussed before). **Figure 8** shows that under NO_2 atmosphere, **P6** becomes doped even during bias stress; while other polymers in the series do not. *This is a unique observation amongst the polymers in this series probably because of the best backbone oxidizability which also reflected as a response of 600% to NO_2 gas.* This observation is exceptional in our series of polymers. For the other polymers **PF1-PF4,** the curves become flat, implying that there is equilibrium between creation of traps by bias stress and filling of traps by NO_2. It therefore seems that bias stress increases the energy level of holes that are trapped by an amount comparable to the range of onset oxidation voltages of **PF1-PF4**, about 0.4 V, which could be viewed as the voltage change across a dipole. (**Table S5, SI**). This built-in dipole requires that a higher electric field be applied to accumulate the same number of charges in a complete layer leading to a shift of V_{th} to more negative values (**Table S5, SI**).[93,94] The reverse bias stress process (the focus of the next results section) lowers the absolute V_{dipole} values and the values are shown in **Table S5, SI**. For the reverse bias stress (trap erase) process, the V_{dipole} values are very small in magnitude which implies a neutralization of trapped charges (**Table S6, SI**).

We next considered the effects of analyte vapors during and after device *recovery* from bias stress. The sequence of experiments was: (i) the polymer active layer is subjected to bias stress (ii) immediately after the bias stress application, the recovery from bias stress is allowed to happen (thereby restoring the original transfer characteristics) with the help of NO_2 gas and the time is monitored (iii) further; the device is exposed to NO_2 for 5 minutes. In another, control experiment, a fresh device with a sensing layer of the same polymer is subjected to the same concentration of the gas for the same time period (5 minutes), the response being recorded and compared.

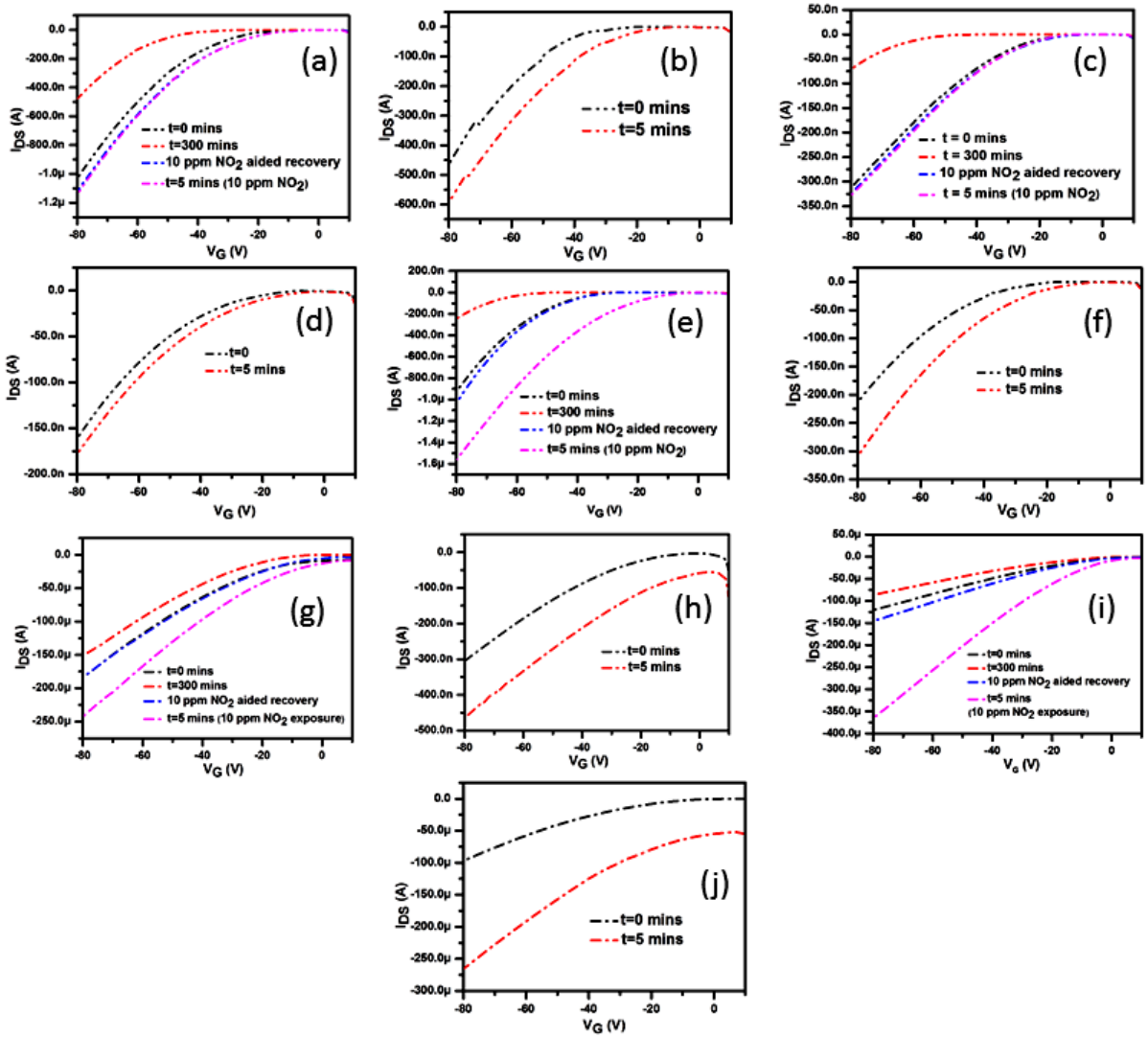

Figure 9. Each plot represents the original transfer curve (t=0 mins), the transfer curve after bias stress (t=300 mins), the transfer curve after recovery from bias stress (10 ppm NO_2 aided); transfer curve on exposure to 10 ppm of NO_2 for 5 minutes after the recovery is complete. The times taken for NO_2 aided recovery are 16±5 mins, 25±2 mins, 18±5, 15±4 mins, 10±4 mins for **PF1-P6** respectively. The responses on 5 minutes of exposure to 10 ppm of NO_2 are written in the main text. The plots are as follows: (a) **PF1** (subjected to gate bias) (b) **PF1** (control, no bias stress, direct exposure) (c) **PF2** (subjected to gate bias) (d) **PF2** (control, no bias stress, direct exposure) (e) **PF3** (control, no bias stress, direct exposure) (f) **PF3** (control, no bias stress, direct exposure)(g) **PF4** (subjected to gate bias) (h) **PF4** (control, no bias stress, direct exposure)(i) **P6** (subjected to gate bias) (j) **P6** (control, no bias stress, direct exposure. Bias stress condition: V_G=V_D=-80 V for 5 hours. Please note that the transfer curve for the best device has been represented; while the times for recovery (for each material **PF1-P6**) have been calculated from an average of 10 devices from different films.

Figure 9 indicates this experiment for V_G=V_D=-80 V. At V_G=V_D=-100 V, we observed an increasing irreversibility; so V_D=V_G=-80 V is a rational choice in terms of a high voltage to conduct stability checks and mechanistic studies. In (a), (c), (e), (g), (i); initial transfer curve (t=0 mins) is indicated by black, the transfer curve immediately after completion of bias stress is indicated in red, the recovery (10 ppm of NO_2 aided) transfer curve in blue and the response

after exposing to 10 ppm of NO_2 for 5 minutes is indicated in pink. It is seen that the response of a device that is subjected to bias stress and made to recover with the aid of NO_2 yields responses close to those of the corresponding control devices (b), (d), (f), (h), (j) for **PF1**, **PF2**, **PF3**, **PF4** and **P6** respectively. Ten devices were measured for the experiment and ten for the controls (**Figure S24, SI**). The finer details are discussed in the figure caption. A t-test was carried out for statistically different means (using the data shown in **Figure 9**) and the results are listed in **Table S7, SI**. The p-values were not significant (confirming the null hypothesis that the means are similar) at $p<0.05$, except for **PF1** and **PF2**. This implies some breakdown for **PF1** and **PF2**. Times taken for trap filling are: 16±5, 25±2, 18±7, and 15±5 and 10±4 minutes respectively for **PF1-PF4** and **P6**. It can be seen that **PF2** and **P6** require the most and least times for trap filling, respectively. The mean responses to NO_2 for the stressed devices are **PF1**:11.8±1.9%, **PF1** control: 14.5±2.6%, **PF2**:6.5±4.4%, **PF2** control: 8.6±3.2%, **PF3**: 52±14%, **PF3** control: 53±18%, **PF4**: 42±20%, **PF4** control: 42±15%, **P6**:160±10%, **P6** control: 162±28%.

In the second case, **Figure S25, SI** reveals the results of the experiment where (i) the polymer active layer is subjected to bias stress (using the same methodologies as described before) (ii) the recovery from bias stress is allowed to proceed in air by keeping in ambient air overnight (~12 hours) (iii) the device is exposed to 10 ppm of NO_2 for 5 minutes. In another control experiment a fresh (unstressed) device with a sensing layer of the same polymer is subjected to the same concentration of the gas for the same time period (5 minutes), with the response recorded and compared. **Figure S25 and S26, SI** indicates this experiment for $V_G=V_D=-80$ V. Ten devices were measured for the experiment and 10 for the controls. The results of the t-test and the p-values obtained are shown in **Table S8, SI**. The p-values are generally insignificant (>0.05 except for **PF2**) which means bias stress does not cause breakdown of devices and the bias stress is reversible. **Figure S27, SI** shows the respective changes in V_{th} and μ on application of bias stress and a complete recovery of these quantities in NO_2 (10 ppm) for all polymers; except in **PF2**. This indicates a degree of instability of sensors based on **PF2**.[37] A degree of instability (drift) for **PF2** was also observed during dynamic bias stress[37] in our previous report that was characterized as the noise. However, the other polymers appear quite stable according to this protocol.

Figure S28, SI shows the transfer curves in air (control) instead of NO_2 (details in the caption). Our study shows that air is not sufficient to induce recovery for **PF1** and **PF2** while for the others sufficient recovery is achieved. The recovery being via an oxidation process is in accordance with the **HOMO** levels/oxidation potentials elucidated via CV studies. The **HOMO** levels of **PF1** and **PF2** were deep, while that of **P6** was found to be closer to vacuum (**Figure S10, SI**) rendering high oxidizability. **PF3** and **PF4** exhibit intermediate recovery. For our

polymer series, the gate-bias stress effect is typically reversible, meaning the trapped charges can be released back into the extended states upon removal of the applied bias. The ΔI_{DS} (%) in the given time is mentioned in the caption of the figure. In air; μ is not changed as much (for **PF3**, **PF4** and **P6**) (**Figure S28, S29, SI**). Further NH_3 exposure (10 ppm) after bias stress (exposure times are mentioned in the **Figure S29, SI** under the figure caption) is unable to create further traps for any the systems (**Figure S29, S30, SI)** which shows unstressed devices exposed to NH_3 (10 ppm) directly; or de-dope the polymer backbone on the same time scale in which a similar exposure to 10 ppm of NO_2 gas was causing complete recovery. Neither the change in V_{th} nor the μ are consistent with further trap creation or de-doping after traps have already been created by bias stress (**Figure S31, SI**).

To summarize, we observe that, as already shown by **CV** studies; **P6** is most capable of stabilizing holes [OS^+ in the SI] which supports our observation that it shows the fastest recovery in air in that fixed amount of time (more details in the figure caption of **Figure 28, SI**). Combining the results on static and dynamic bias stress in our current and previous work, we find that (i) **P6** has the fastest trap equilibrium; but may not be the best option to get stability in air (ii) **PF4** has a relatively smaller τ value unlike **P6** showing slower trap equilibrium; but had the highest D value by virtue of lower drifts (iii) The rates of decrease of currents at V_G=-80 V due to environmental drift (dynamic bias stress)~10^{-4}-10^{-5} [37] while the rates ($k=1/\tau$) for static bias stress are comparable, ~10^{-5} s^{-1} indicating substantial stability to both. This also shows that only a small proportion of the traps induced during the forward sweeps in dynamic bias stress are removed during the immediately following reverse sweeps.[37]

Trap erasing/electrostatic doping/reverse bias stress effects on vapor responses. De-trapping of holes explains the positive shift in V_{th} towards the initial values during recovery from bias stress. We now induce a further detrapping process, erasing not only the traps created during bias stress but also those originally present, and investigate the responses of such devices to vapors. We obtained an enhanced response to NH_3 after reverse bias stress. We used the following protocol in 4 independent experiments: (i) trap erase followed by (ii) 10 ppm of NO_2 exposure; (ii) exposure to 10 ppm of NH_3 or (iii) ambient air, as control (**Figure S32, SI**). Details are explained in the caption. If positive bias stress is applied, electron trapping/hole detrapping occurs at the gate-insulator/active-layer interface; resulting in the shifting of V_{th} farther to the positive gate voltage direction.[95] We have used the charging method to observe steady and large positive V_{th} shifts when applying V_G = +80V and V_D=0 V, after the prior application of negative bias stress to create traps; which are then erased by the positive gate bias.[95,49] The bias stress protocol (V_G=V_D=-80 V, 2.5 hours) was applied first, followed by the erase protocol (V_G=-80 V, V_D=0 V, 2.5 hours). Note that in our earlier experiments, the bias

stress was applied for 5 hours. In this case (erase), the bias stress voltages (gate and drain) were applied for 2.5 hours and all traps (defects) were erased for 2.5 hours. Changes are all similar irrespective of the nature of the polymer backbone electronic structure/microstructure, implying that the charges are accumulated in the dielectric.[82] **Table S9, SI** shows no correlation of ΔV_{th} and $\Delta\mu$ with the backbone oxidation potentials; the drain current increases however follow the backbone oxidation potentials.

The trap-erase experiment is relevant to **OFET** sensors to verify the mechanism of vapor response by unstressed devices. Independent devices had traps erased by the charging process and then exposed to (i) NO_2 (10 ppm) (ii) NH_3 (10 ppm) and (iii) air. The exposure times are 16, 25, 18, 15, 10 minutes for **PF1-PF4** and **P6**, respectively. NO_2 does not significantly dope further after traps are filled by the electric field (**Figure S32, SI,** showing ΔV_{th} and $\Delta\mu$ (%)). This is true for all the polymers. I_{DS} follows the trend **P6>PF4>PF3>PF2>PF1** (**Figure S33, SI**). Moreover, the injected charge $q_{injected}$ is similar for all samples as $q=C_{ox}\Delta V_{th}$. *The response to NH_3 after trap erase is greater than for direct NH_3 exposure without trap erase.* The response to NH_3 is compared to the natural recovery (**Figure 10**) post trap erase and it is observed that responses to NH_3 are larger compared to recovery on exposure to air for the same amount of time, post trap erase. The response was highest for **PF2** and **PF3**, while **PF1**, **PF4** and **P6** show similar responses to each other. **P6** shows similar response (ΔI_{DS} %) to air and 10 ppm of NH_3 which implies that additional injected mobile holes in **P6** are easily re-trapped in air. **PF4** also shows a similar trend. But as discussed above, NH_3 promotes complete recovery and restoration of more negative V_{th} (**Figure S34, SI**). The NH_3 current response (in unbiased devices), and responses to air and NH_3 post trap erase are shown in **Figure S36, S37, SI**. ΔV_{th} and $\Delta\mu$ (%) after trap erase, the response controls (transfer curves, unbiased devices, with and without NH_3 exposure) point to the fact that trap-erasing increased the responses of all five polymers to NH_3 , which relates the responses to a trap-creation process. Also, the fact that this occurred for polymers with a range of onset oxidation voltages of about 0.5 V indicates that the reverse bias stress changed the minimum mobile hole energy level by at least that amount.

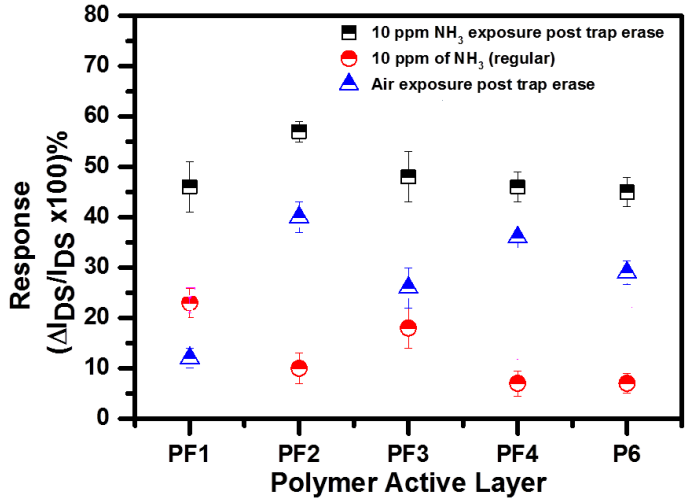

Figure 10. A comparison of responses (V_G=-80 V) to 10 ppm of NH_3 (i) post electrostatic doping or trap erase (ii) an independent (unstressed) device being exposed to 10 ppm of NH_3 directly (iii) exposure of an electrostatically doped device to air (control). The exposure times are 16 mins for **PF1**, 25 mins for **PF2**, 18 mins for **PF3**, 15 mins for **PF4** and 10 mins for **P6**.

Conclusions

We have definitively established the major role of traps in the vapor sensing mechanism of a series of five air-stabilized *p*-channel conjugated polymers. All but one of the polymers show good recovery from bias stress even at very high operational voltages, such as -80 V, meaning that the responses to vapors are reproducible after a bias stress-recovery cycle. Furthermore, the sensitivities of three of the polymers to NO_2 acting as a dopant are highly reproducible after recovery either accelerated by NO_2 as a trap filler or in the ambient air; the exceptions exhibit conformational and packing defects and high free volume.[37]

In our previous work, two of the polymers had shown high signal/drift ratios "D" for NO_2 exposure; one of them (**P6)** due to exceptionally high response and good oxidizability while the other (**PF4)** due to lower drift under dynamic bias stress. We also showed that vapor response is independent of the channel length. We analysed the bias stress of the unexposed polymers in terms of trap distribution and a stretched exponential approach to shifted V_{th}. While **P6** showed the fastest recovery from bias stress and the narrowest trap energy distribution, the more moderate recovery rate and trap energy distribution of **PF4** may have aided its environmental stability. Finally, we showed that response to NH_3 is a trap-creation process by applying reverse bias stress; this increased the response to NH_3 as traps are refilled, while response to NO_2 under this condition was negligible as the reverse bias stress set a mobile carrier energy level beyond the capability of NO_2 for further doping. This suggests that reverse bias stress can prime an OFET sensor for an immediate enhanced response to a trap-creating vapor analyte.

Acknowledgments. We thank Justine Wagner and Evan Plunkett for helpful discussions. This work was supported by the National Science Foundation, ECCS Division, Award Number 1807293.

References

(1) T. Dalhamn and J. Sjöholm, *Acta Physiol. Scand.* , 1963**, 58,** 287-291.

(2) C. Zhang, P. Chen and W. Hu, *Chem. Soc. Rev*. 2015, **44**, 2087-2107.

(3) S. S. Varghese, S. Lonkar, K. K. Singh, S. Swaminathan and A. Abdala, *Sens. Actuators B*

Chem., 2015, **218**, 160-183. https://doi.org/10.1016/j.snb.2015.04.062.

(4) J. Li, Y. Lu, Q.Ye, M. Cinke, J. Han and M. Meyyappan, *Nano Lett.* 2003**, 3**, 929-933.

(5) J. Kong, N. R. Franklin, C. Zhou, M. G. Chapline, S. Peng, K. Cho and H. Dai, *Science,* 2000**, 287,** 622-625.

(6) K. Wetchakun, T. Samerjai, N. Tamaekong, C. Liewhiran, C. Siriwong, V. Kruefu, A. Wisitsoraat, A. Tuantranont and S. Phanichphant, *Sens. Actuator B Chem.,* 2011, **160**, 580-591. https://doi.org/10.1016/j.snb.2011.08.032.

(7) S. Yang, C. Jiang and S. huai. Wei, *Appl. Phys. Rev*., 2017, **4**, 021304. https://doi.org/10.1063/1.4983310.

(8) G. Korotcenkov, V. Brinzari and M. H. Ham, *Key Eng. Mater.,* 2018, **780**, 80-89.

(9) X. Liu, S. Cheng, H. Liu, S. Hu, D. Zhang and H. Ning, *Sensors,* 2012, **12**, 9635-9665.

(10) J. Dai, O. Ogbeide, N. Macadam, Q. Sun, W. Yu, Y. Li, B. L. Su, T. Hasan, X. Huang and W. Huang, *Chem. Soc. Rev.,* 2020, **49**, 1576-1589.

(11) R. Song, Z. Wang, X. Zhou, L. Huang and L. Chi, *ChemPlusChem*., 2019, **84**, 1222-1234.

(12) S. H. Yu, J. Cho, K. M. Sim, J. U. Ha and D. S. Chung, *ACS Appl. Mater. Interfaces,* 2016**, 8**, 6570-6576.

(13) L. Dai, P.Soundarrajan and T. Kim, *Pure Appl. Chem.,* **2002**, 74, 1753-1772.

(14) S. Feng, F. Farha, Q. Li, Y. Wan, Y.; Xu, T. Zhang and H. Ning, *Sensors,* 2019, **19**, 3760. https://doi.org/10.3390/s19173760.

(15) J. W. Grate, *Chem. Rev*., 2008, **108**, 726-745.

(16) J. Wagner, H. J. Jang, J. Han and H. E. Katz, *Mater. Horiz.,* 2020**, 7**, 1358-1371.

(17) J. Zhou, H. Lin, X. F. Cheng, J. Shu, J. H. He, H. Li, Q. F. Xu, N. J. Li, D. Y. Chen and J. M. Lu, *Mater. Horiz.,* 2019**, 6**, 554-562.

(18) C. F. Lu, C. W. Shih, C. A. Chen, A. Chin and W. F. Su, *Adv. Funct. Mater.,* 2018, **28**, 1803145. https://doi.org/10.1002/adfm.201803145.

(19) M. Kaur, D. K. Aswal and J. V. Yakhmi, *Science and Technology of Chemiresistor Gas Sensors*, 2007, 33-93.

(20) R. Alrammouz, J. Podlecki, P. Abboud, B. Sorli and R. Habchi, *Sens. Actuator A Phys*., 2018, **284**, 209-231.

(21) S. Badhulika, N. V. Myung and A. Mulchandani, *Talanta,* 2014, **123**, 109-114.

(22) S. Tiwari, W. Takashima, S. K. Balasubramanian, S. Miyajima, S. Nagamatsu, S. S.Pandey and R. Prakash, *Jpn. J. Appl. Phys.,* 2014**,** **53**, 021601. https://doi.org/10.7567/JJAP.53.021601.

(23) M. Sainato, L. M. Strambini, S. Rella, E. Mazzotta and G. Barillaro, *ACS Appl. Mater. Interfaces,* 2015, **7**, 7136-7145.

(24) D. Sarkar, H. Gossner, W. Hansch and K. Banerjee, *Appl. Phys. Lett.,* 2013, **102**, 023110. https://doi.org/10.1063/1.4775358.

(25) Z. Song, G. Liu, Q. Tang, X. Zhao, Y.Tong and Y. Liu, *Org. Electron.,* 2017, **48**, 68-76.

(26) J. H. Lee, Y. Seo, Y. D. Park, J. E. Anthony, D. H. Kwak, J. A. Lim, S. Ko, H. W. Jang, K. Cho and W. H. Lee, *Sci. Rep.,* 2019, **9**. https://doi.org/10.1038/s41598-018-36652-1.

(27) H. Fei, G. Wu, W. Y. Cheng, W. Yan, H. Xu, D. Zhang, Y. Zhao, Y. Lv, Y. Chen and L. Zhang, *ACS Omega,* 2019, **4**, 3812-3819.

(28) T. N. Ly and S. Park, *Sci. Rep.,* 2018, **8**, 18030. https://doi.org/10.1038/s41598-018-36468-z.

(29) W. K. Jang, J. Yun, H. I. Kim and Y. S. Lee, *Colloid Polym. Sci.,* 2013, **291**, 1095-1103.

(30) K. H. Cheon, J. Cho, Y. H. Kim and D. S. Chung, *ACS Appl. Mater. Interfaces,* 2015, **7**, 14004-14010.

(31) T. Xie, G. Xie, Y. Zhou, J. Huang, M. Wu, Y. Jiang and H. Tai, *Chem. Phys. Lett.,* 2014, ***614*****,** 275-281.

(32) L. Wang, S. Chen, W. Li, K. Wang, Z. Lou and G. Shen, *Adv. Mater.,* 2019, **31**, 1804583. https://doi.org/10.1002/adma.201804583.

(33) X. Wang, S.S. Yee and W.P. Corey, *Sens. Actuators B Chem.,*1995, **25**, 454-457.

(34) K. Yang, W. Yuan, Z. Hua, Y. Tang, F. Yin and D. Xia, *ACS Appl. Mater. Interfaces,* 2020, **12**, 3919-3927.

(35) T. Marszalek, M. Li and W. Pisula, *Chem. Commun.,* 2016, **52**, 10938-10947.

(36) K. Mahesh, S. Karpagam and K. Pandian, *Top. Curr. Chem.,* 2019, ***377:12.*** https://doi.org/10.1007/s41061-019-0237-4.

(37) T. Mukhopadhyaya, J. S. Wagner, H. Fan and H. E. Katz, *ACS Appl. Mater. Interfaces,* 2020, **12**, 21974-21984.

(38) Y. Yang, G. Zhang, H. Luo, J. Yao, Z. Liu and D. Zhang, *ACS Appl. Mater. Interfaces,* 2016, **8**, 3635-3643.

(40) X. Zhang, B. Wang, L. Huang, W. Huang, Z. Wang, W. Zhu, Y. Chen, Y. L. Mao, A. Facchetti and T. J. Marks, *Sci. Adv.*, 2020. https://doi.org/10.1126/sciadv.aaz1042.

(41) K. Besar, S. Yang, X. Guo, W. Huang, A. M. Rule, P. N. Breysse, I. J. Kymissis and H. E. Katz, *Org. Electron.,* 2014, **15**, 3221-3230.
(42) L. Feng, W. Tang, J. Zhao, R. Yang, W. Hu, Q. Li, R. Wang and X. Guo, *Sci. Rep.,* 2016, **6**, 20671. https://doi.org/10.1038/srep20671.

(43) Z. Yang, S. Han, Y. Liu, X. Zhuang, D. Akinwande and J. Yu, *Org. Electron.,* 2018, **62**, 114-120.
(44) Y. C. Wong, B. C. Ang, A. S. M. A. Haseeb, A. A. Baharuddin and Y. H. Wong, *J. Electrochem. Soc.,* 2020, **167**, 037503. https://doi.org/10.1149/2.0032003jes.

(45) H. F. Haneef, A. M. Zeidell and O. D. Jurchescu, *J. Mater. Chem. C*., 2020, **8**, 759-787.

(46) S. V. Novikov, *J. Polym. Sci. Part B: Polym. Phys.,* 2003, **41**, 2584-2594.

(47) W. Huang, W. Shi, S. Han and J. Yu, *AIP Adv.,* 2013, **3**, 052122. https://doi.org/10.1063/1.4807660.

(48) D. Abbaszadeh, A. Kunz, N. B. Kotadiya, A. Mondal, D. Andrienko, J. J. Michels, G. J. A. H. Wetzelaer and P. W. M. Blom, *Chem. Mater.*, 2019, **31**, 6380-6386.

(49) Q. Zhang, T. S. Kale, E. Plunkett, W. Shi, B. J. Kirby, D. H. Reich and H. E. Katz, *Macromolecules,* 2018, **51**, 6011-6020.

(50) R. Schmechel and H. Von Seggern, *Phys. Status Solidi Appl. Res.,* 2004, **201**, 1215-1235. https://doi.org/10.1002/pssa.200404343.

(51) L. G. Kaake, P. F. Barbara and X. Y. Zhu, *J. Phys. Chem. Lett.,* 2010**, 1**, 628-635.

(52) H. H. Choi, W. H. Lee and K. Cho, *Adv. Funct. Mater.,* 2012, **22**, 4833-4839.

(53) Y. J. Jeong, D. J. Yun, S. Nam and J. Jang, *Appl. Surf. Sci.,* 2019, **481**, 642-648.

(54) W. H. Lee, H. H. Choi, D. H. Kim and K. Cho, *Adv. Mater.,* 2014, **26**, 1660-1680.
(55) S. Park, S. H. Kim, H. H. Choi, B. Kang and K. Cho, *Adv. Funct. Mater.,* 2020, **30**, 1904590. https://doi.org/10.1002/adfm.201904590.

(56) B. Kang, B. Moon, H. H. Choi, E. Song and K. Cho, *Adv. Electron. Mater.,* 2016, **2**, 1500380. https://doi.org/10.1002/aelm.201500380.

(57) W. Huang, X. Zhuang, F. S. Melkonyan, B. Wang, L. Zeng, G. Wang, S. Han, M. J. Bedzyk, J. Yu and T. J. Marks, *Adv. Mater.,* 2017, **29**, 1701706. https://doi.org/10.1002/adma.201701706.

(58) P. Lin and F. Yan, *Adv. Mater.,* 2012, **24,** 34-51.

(59) Z. Yuan, R. Li, F. Meng, J. Zhang, K. Zuo and E. Han, *Sensors,* 2019, **19**, 1495. https://doi.org/10.3390/s19071495.

(60) A. M. Andringa, C. Piliego, I. Katsouras, P. W. M. Blom and D. M. D. Leeuw, *Chem. Mater.,* 2016, **26**, 773-785.

(61) A. Pogantsch, N. Zaami and C. Slugovc, *Chem. Phys.,* 2006, **322,** 399-404.
(62) K. Becker, J. M. Lupton, J. Feldmann, B. S. Nehls, F. Galbrecht, D. Gao and U. Scherf, *Adv. Funct. Mater.,* 2006, **16,** 364-370.
(63) S. B. Darling, *J. Phys. Chem. B,* 2008, **112,** 8891-8895.
(64) S. Hayashi, S. Inagi and T. Fuchigami, *Polym. J.,* 2010, **42**, 772-775.
(65) S. H. Chen, A. C. Su and S. A. Chen, *J. Phys. Chem. B,* 2005, **109,** 10067-10072.
(66) H. J. Eggimann, F. L. Roux and L. M. Herz, *J. Phys. Chem. Lett.* 2019, **10**, 729–1736
(67) Y. Yang, Z. Liu, Z., J. Chen, Z. Cai, Z. Wang, W. Chen, G. Zhang, X. Zhang, L. Chi and D. A. Zhang, *Adv. Sci.,* 2018, **5,** 1801497. https://doi.org/10.1002/advs.201801497.
(68) J. Ma, Z. Liu, Z. Wang, Y. Yang, G. Zhang, X. Zhang and D. Zhang, *Mater. Chem. Front.,* 2017, **1,** 2547-2553.
(69) S. Kappaun, C. Slugovc and E. J. W. List, *Adv. Polym. Sci.* 2008, **212**, 273-294.
(70) P. A. Bobbert, A. Sharma, S. G. J. Mathijssen, M. Kemerink and D. M. De Leeuw, *Adv. Mater.,* 2012, **24**, 1146-1158.

(71) W. Tang, J. Zhao, Y. Huang, L. Ding, Q. Li, J. Li, P. You, F. Yan and X. Guo, *IEEE Electron Device Lett.,* 2017, **38**, 748-751.

(72) W. Tang, J. Zhao, Y. Huang, L. Ding, S. Chen and X. Guo, *7th International Conference on Computer Aided Design for Thin-Film Transistor Technologies, CAD-TFT,* 2016. https://doi.org/10.1109/CAD-TFT.2016.7785044.
(73) D. K. Hwang, K. Lee, J. H. Kim, S. Im, J. H. Park and E. Kim, *Appl. Phys. Lett.,* 2006, **89**, 093507.

(73) Y. R. Liu, R. Liao, P. T. Lai, R. H. Yao, *IEEE Trans. Device Mater. Reliab.*, 2012*,* **12.** https://doi.org/10.1109/TDMR.2011.2163408.

(74) O. Knopfmacher, M. L. Hammock, A. L. Appleton, G. Schwartz, J. Mei, T. Lei, J. Pei and Z. Bao, *Nat. Commun.*, 2014, **5**, 2954. https://doi.org/10.1038/ncomms3954.

(75) T. Mukhopadhyay, B.P. Puttaraju, S. Senanayak, A. Sadhanala, R. A. Friend, H. D. Faber, T. Anthopoulos, U. Salzner, A. Meyer and S. Patil, *ACS Appl. Mater. Interfaces,* **2016**, *8*, 25415–25427.

(76) S. G. J. Mathijssen, M. Cölle, H. Gomes, E. C. P. Smits, B. De Boer, I. McCulloch, P. A. Bobbert and D. M. De Leeuw, *Adv. Mater.,* 2007, **19**, 2785-2789.

(77) Y. X., Li, H. Zhang, M. N. Yu, S. S. Wang, Y. R. Liu, D. Q. Lin, L. H. Xie, Z. Q. Lin and W. Huang, W. *Nanoscale* 2019, **50**, 5298-5307.
(78) J. U., Wallace and S. H. Chen, *Adv. Polym. Sci.,* 2008, **212**, 145-186.
(79) Z. Chen, M. J. Lee, R. Shahid Ashraf, Y. Gu, S. Albert-Seifried, M. Meedom Nielsen, B. Schroeder, T. D. Anthopoulos, M. Heeney and I. McCulloch, *Adv. Mater.,* 2012, **24**, 647-

652.
(80) C. Goldmann, C. Krellner, K. P. Pernstich, S. Haas, D. J. Gundlach and B. Batlogg, *J. Appl. Phys.* 2006, **99**, 034507. https://doi.org/10.1063/1.2170421.

(81) W. L. Kalb and B. Batlogg, *Phys. Rev. B,* 2010, **81**, 035327. https://doi.org/10.1103/PhysRevB.81.035327.

(82) S. G. J. Mathijssen, M. J. Spijkman, A. M. Andringa, P. A. Van Hal, I. McCulloch, M. Kemerink, R. A. J. Janssen and D. M. De Leeuw, *Adv. Mater.* 2010, **22**, 5105-5109.

(83) K. Keunen, A. Stesmans and V. V. Afanas'Ev, *Phys. Rev. B,* 2011, **84**, 085329. https://doi.org/10.1103/PhysRevB.84.085329.

(84) B. J. O'Sullivan, P. K. Hurley, C. Leveugle and J. H. Das, *J. Appl. Phys.,* 2001, **89**, 3811. https://doi.org/10.1063/1.1343897.

(85) I. Vladimirov, M. Kühn, T. Geßner, F. May and R. T. Weitz, *Sci. Rep.,* 2018, **8:14868.** https://doi.org/10.1038/s41598-018-33308-y.

(86) G. Blatter and F. Greuter, *Phys. Rev. B,* 1986, **34.** https://doi.org/10.1103/PhysRevB.34.8555.

(87) A. van den Beukel and J. Sietsma, *Acta Metall. Mater.* 1990, **38**, 383-389.
(88) M. L., Cheng and Y. M. Sun, *Polymer,* 2009, **50,** 5298-5307.
(89) K. K. Ryu, I. Nausieda, D. Da He, A. I. Akinwande, V. Bulović and C. G. Sodini, *IEEE Trans. Electron Devices,* 2010, **57**, 1003-1008.

(90) D. K. Schroder, *Microelectron. Reliab.,* 2007, **47**, 841-852.

(91) H. H. Choi, M. S. Kang, M. Kim, H. Kim, J. H. Cho and K. Cho, *Adv. Funct. Mater.*,2013, **23**, 841-852.

(92) J. Lee, H. Min, N. Park, H. Jeong, S. Han, S. H. Kim and H. S. Lee, *ACS Appl. Mater. Interfaces,* 2015, **7***,* 25045-25052.

(93) M. Salinas, C. M. Jäger, A. Y. Amin, P. O. Dral, T. Meyer-Friedrichsen, A. Hirsch, T. Clark and M. Halik, *J. Am. Chem. Soc.,* 2012, **134**, 12648-12652.

(94) M. Aghamohammadi, R. Rödel, U. Zschieschang, C. Ocal, H. Boschker, R. T. Weitz, E. Barrena and H. Klauk, *ACS Appl. Mater. Interfaces,* 2015, **7**, 22775-22785.

(95) K. D. Deshmukh, J. E. West and H. E. Katz, , *Proceedings - International Symposium on Electrets*, 2008. https://doi.org/10.1109/ISE.2008.4814032.